

Model-Independent Z' Constraints from Measurements at the Z Peak

A. Leike¹

Ludwigs-Maximilians-Universität, Sektion Physik, Theresienstr. 37,
D-80333 München, Germany
E-mail: leike@graviton.hep.physik.uni-muenchen.de

Abstract

Model independent constraints on extra neutral gauge bosons are obtained from partial decay widths of the Z_1 and forward-backward and left-right asymmetries at the Z_1 peak. Constraints on the ZZ' mixing angle in E_6 models are considered as special cases.

The measurements at the Z_1 resonance at LEP 1 are in very good agreement with the SM. This agreement can be interpreted as a constraint on new physics. In particular, the experiments at LEP 1 give the best present constraints on the ZZ' mixing angle θ_M [1, 2]. Because these constraints depend on the couplings of the Z' to SM fermions, they are usually given for selected Z' models. Typical allowed regions for θ_M in E_6 models are $-0.005 < |\theta_M| < 0.003$ at the 95% CL, see [3]. In these *model dependent* analyses, all couplings of the Z' to the SM fermions are linked by model assumptions.

Model dependent Z' analyses have the advantage that many observables can be used as input for the fit. Furthermore, the resulting Z' constraints can easily be compared with other experiments. They have the disadvantage that the output is a mixture of experimental data and theoretical assumptions. For every model, a separate fit has to be performed.

A *model independent* Z' analysis does not rely on model assumptions. It can constrain only certain *combinations* of Z' parameters. Model dependent Z' constraints can be obtained from model independent Z' constraints as special cases.

For a complete analysis, *model dependent* analyses should be complemented by a *model independent* analysis. Such a model independent Z' analysis is done for off-resonance fermion pair production [4, 5] and W pair production [6] at future e^+e^- colliders. A model independent Z' analysis for fermion pair production based on present LEP 2 data also exists [3]. It is not yet performed for LEP 1 data.

In this paper, we show how a model independent Z' analysis based on LEP 1 data could be done using the partial decay widths of the Z_1 and forward-backward and left-right asymmetries at the Z_1 peak as input.

¹Supported by the EC-program CHRX-CT940579

To fix the notation, we repeat the neutral current interaction with SM fermions,

$$\mathcal{L} = eA_\mu J_\gamma^\mu + gZ_\mu J_Z^\mu + g'Z'_\mu J_{Z'}^\mu, \quad J_{Z'}^\mu = \sum_f \bar{f} \gamma^\beta (v'_f + \gamma^5 a'_f) f. \quad (1)$$

Denoting the symmetry eigenstates by Z and Z' , the mass eigenstates Z_1 and Z_2 are given by mixing,

$$Z_1 = Z \cos \theta_M + Z' \sin \theta_M, \quad Z_2 = -Z \sin \theta_M + Z' \cos \theta_M. \quad (2)$$

In the following, we are interested in the light mass eigenstate Z_1 precisely studied at LEP 1. Its axial vector and vector couplings to SM fermions depend on the ZZ' mixing angle θ_M ,

$$a_f(1) = a_f \cos \theta_M + \frac{g'}{g} a'_f \sin \theta_M, \quad v_f(1) = v_f \cos \theta_M + \frac{g'}{g} v'_f \sin \theta_M. \quad (3)$$

The eigenvalue equation relates the mixing angle and the masses of the symmetry and mass eigenstates,

$$\frac{M_Z^2}{M_1^2} = \rho_{mix} = 1 + \sin^2 \theta_M \left(\frac{M_2^2}{M_1^2} - 1 \right). \quad (4)$$

Consider the partial decay width Γ_1^f of the Z_1 to $f\bar{f}$ and the forward-backward and left-right asymmetries at the peak in the limit of small ZZ' mixing,

$$\begin{aligned} \Gamma_1^f &= M_1 \frac{g^2}{12\pi} [v_f^2(1) + a_f^2(1)] N_f \approx \Gamma_1^{f0} \left\{ 1 + 2 \frac{v_f v_f^M + a_f a_f^M}{g(v_f^2 + a_f^2)} \right\}, \\ A_{FB}^f &= \frac{3}{4} A_e A_f \approx A_{FB}^{f0} + \frac{3}{4} A_f^0 \Delta A_e + \frac{3}{4} A_e^0 \Delta A_f, \\ A_{LR}^f &= A_f \approx A_f^0 + \Delta A_f \end{aligned} \quad (5)$$

$$\text{with } A_f \equiv \frac{2a_f(1)v_f(1)}{a_f(1)^2 + v_f(1)^2}, \text{ and } \Delta A_f \approx 2 \frac{v_f a_f^M + a_f v_f^M}{g(v_f^2 + a_f^2)} - 4 \frac{a_f^2 v_f a_f^M + v_f^2 a_f v_f^M}{g(v_f^2 + a_f^2)^2}. \quad (6)$$

The index zero denotes the observables without mixing. We see that measurements at the Z_1 peak constrain the combinations a_f^M and v_f^M ,

$$a_f^M \equiv \theta_M g' a'_f, \quad v_f^M \equiv \theta_M g' v'_f, \quad (7)$$

and not a'_f, v'_f and θ_M separately. For example, the observables with only leptons in the final state, Γ_1^l , A_{FB}^l and A_{LR}^l , give model independent constraints on a_l^M and v_l^M . Neglecting correlations, they are

$$\begin{aligned} |C_v^l v_l^M + C_a^l a_l^M| &< \frac{\Delta \Gamma_1^l}{\Gamma_1^l}, \\ |D_v^l v_l^M + D_a^l a_l^M| &< \Delta A_l, \\ |E_v^l v_l^M + E_a^l a_l^M| &< \Delta A_{FB}^l. \end{aligned} \quad (8)$$

The coefficients $C_{v,a}^l, D_{v,a}^l$ and $E_{v,a}^l$ depend on SM parameters only and can be easily deduced from equations (5). The right hand side of the inequalities (8) are experimental errors.

Model independent limits for a_f^M, v_f^M , $f = q$ can be obtained in a similar way with the exception that A_{FB}^f depends on the leptonic couplings too. We are interested in two-dimensional

constraints on a_f^M and v_f^M . Therefore, we interpret the constraint from A_{FB}^f as a second measurement of A_f ,

$$A_f = \frac{4}{3} \frac{A_{FB}^f}{A_e}, \quad \Delta A_f = \frac{4}{3} \frac{\sqrt{(\Delta A_{FB}^f A_e^0)^2 + (A_{FB}^{f0} \Delta A_e)^2}}{(A_e^0)^2}. \quad (9)$$

To get the connection to real data, radiative corrections have to be taken into account. They modify the relations (8) estimated at the Born level. Electroweak corrections can be included interpreting a_f and v_f in equation (3) contributing to $a_f(1)$ and $v_f(1)$ as effective couplings. Using the effective Weinberg angle $\sin^2 \theta_W^{eff} = 0.2317$, excellent agreement with the theoretical predictions in table 2 of [7] is obtained for $\theta_M = 0$:

| | | | | | | | |
|----------------------------------|--------|------------|-------|------------|-------|------------|------|
| observable | A_l | A_{FB}^l | A_c | A_{FB}^c | A_b | A_{FB}^b | |
| [7] | 0.1457 | 0.0159 | 0.667 | 0.0729 | 0.933 | 0.1020 | |
| $\sin^2 \theta_W^{eff} = 0.2317$ | 0.1456 | 0.0159 | 0.667 | 0.0728 | 0.935 | 0.1022 | |
| experimental errors, [8] | 0.0067 | 0.0010 | 0.084 | 0.0048 | 0.049 | 0.0023 | (10) |

We included the electroweak [9] and QCD corrections for Γ_1^f following [10],

$$\Gamma_1^f = \frac{N_f G_\mu \sqrt{2} M_1^3}{12\pi} \rho_{mix} \rho_f^Z \mu R_{\text{QED}} R_{\text{QCD}}(M_1^2) \left\{ [v_f(1)^2 + a_f(1)^2] \left(1 + 2 \frac{m_f^2}{M_1^2} \right) - 6 a_f(1)^2 \frac{m_f^2}{M_1^2} \right\}, \quad (11)$$

where

$$\begin{aligned} R_{\text{QED}} &= 1 + \frac{3}{4} \frac{\alpha}{\pi} Q_f^2, \quad \mu = \sqrt{1 - \frac{4m_f^2}{M_1^2}}, \\ R_{\text{QCD}} &= 0 \quad \text{for } f = l, \\ R_{\text{QCD}} &= 1 + \frac{\alpha_s(M_1^2)}{\pi} + 1.405 \frac{\alpha_s^2(M_1^2)}{\pi^2} - 12.8 \frac{\alpha_s^3(M_1^2)}{\pi^3} - \frac{Q_f^2 \alpha \alpha_s(M_a^2)}{4 \pi^2} \quad \text{for } f = q. \end{aligned} \quad (12)$$

In contrast to [10], we use the normalization $a_l = -\frac{1}{2}$. For Γ_1^b , additional contributions must be taken into account, see [7, 10] for original references.

Note that the coupling g^2 in equation (5) has to be replaced by G_μ to meet the experimental accuracy,

$$g^2 = \frac{4\pi\alpha}{\sin^2 \theta_W \cos^2 \theta_W} = \frac{G_\mu \sqrt{2} M_Z^2}{1 - \Delta r} = \frac{G_\mu \sqrt{2} M_W^2}{(1 - \Delta r) \cos^2 \theta_W}, \quad (13)$$

where Δr is absorbed in ρ_f^Z . The last of the above sequence of equations is valid only for restricted Higgs sectors. Through this replacement, a dependence on the Z mass, M_Z , appears. Unfortunately, this induces, through equation (4), a dependence of Γ_1^f on M_Z , which was absent at the Born level. For model independent limits on a_f^M and v_f^M , this dependence can be eliminated by additional experimental input. The knowledge of M_W , G_μ and $\alpha(M_Z^2)$ together with equation (13) allows to calculate M_Z for models with restricted Higgs sectors. The main error of the calculated value of M_Z comes from the experimental error of the M_W measurement [8] and from the theoretical uncertainty of Δr due to the unknown Higgs and top mass [11]. We add these errors quadratically. As a result, we get $\rho_{mix} = M_Z^2/M_1^2 = 1 \pm 0.003$. We have $\rho_{mix} > 1$ in a theory with a Z' . Note that the data used for the calculation of ρ_{mix} are independent of the measurements used for our further Z' analysis. We include the *shift* of

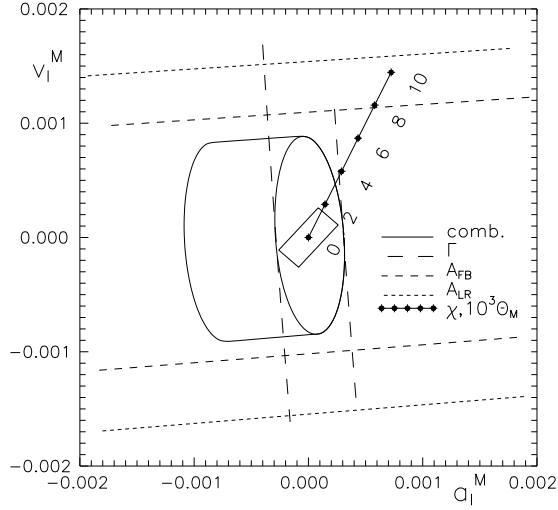


Fig. 1: Areas of (a_l^M, v_l^M) , for which the extended gauge theory's predictions are indistinguishable from the SM (95% CL). Models between the long-dashed (short-dashed, dotted) lines cannot be detected with Γ_1^l (A_{FB}^l, A_{LR}^l). The regions surrounded by the solid lines cannot be resolved by all three observables combined, see text. The numbers at the straight line indicate the value of θ_M in units of 10^{-3} for the χ model. The rectangle is calculated from figure 1 of reference [6].

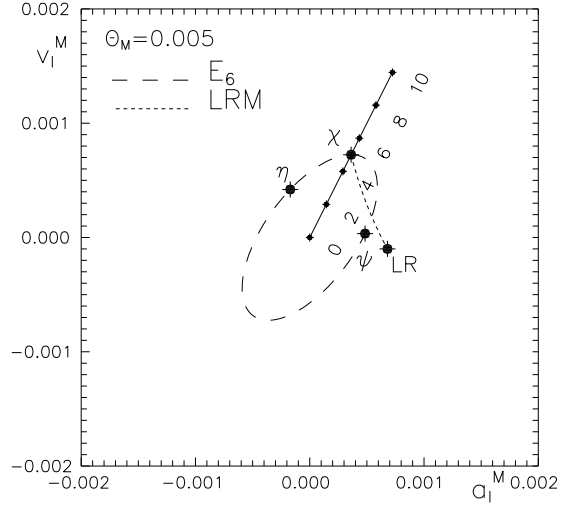


Fig. 2: The vector and axial vector couplings a_l^M, v_l^M for $\theta_M = 0.005$ in typical GUTs. For illustration, θ_M for the χ model is varied in units of 10^{-3} .

ρ_{mix} from 1, which is within the experimental errors, in ρ_f^Z . The error of ρ_{mix} is included in the error of Γ_1^f .

Figure 1 illustrates the constraints on a_l^M and v_l^M . The plotted regions correspond to $\chi^2 = 5.99$. In our demonstration, the central value of the fit is assumed to be at the theoretical prediction but the experimental error quoted in (10) is used. We use $\Gamma_1^l = (83.91 \pm 0.11) \text{ MeV}$ [8] as input. Fixing $\rho_{mix} = 1$, the region inside the ellipse cannot be excluded by the data. The constraint from every observable is shown separately for $\rho_{mix} = 1$. The uncertainty of ρ_{mix} yields to a shift of the ellipse, which results to the larger solid region in figure 1. Future improved measurements of M_W and a determination of M_H would reduce the difference between the two regions.

The *model independent* constraints can be interpreted as constraints to the ZZ' mixing angle θ_M for any fixed model. This is illustrated for the χ model in figure 1. Graphically, one obtains $|\theta_M| < 0.0035$.

Similarly, the constraints on θ_M could be obtained for any other model. This is illustrated in figure 2, where a_l^M, v_l^M for E_6 models [12, 13] and left-right models [13, 14] with $\theta_M = 0.005$ are shown. A superposition with figure 1 allows to obtain the limits on θ_M for any E_6 and left-right model. The constraints for the η, ψ and LR model are $|\theta_M| < 0.01, 0.0035$ and 0.0025 , correspondingly.

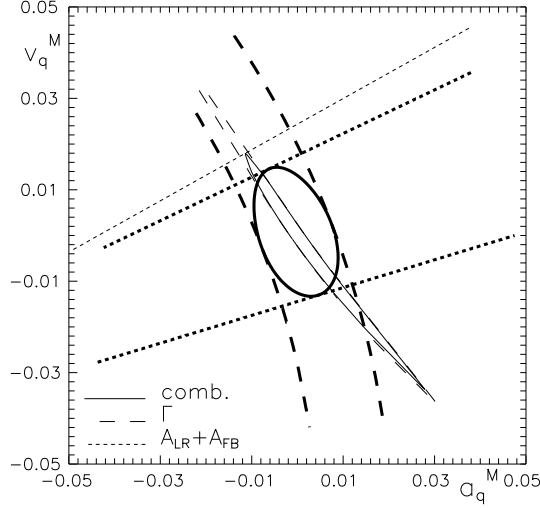


Fig. 3: Areas of (a_q^M, v_q^M) , for which the extended gauge theory's predictions are indistinguishable from the SM (95% CL). Models between the dashed (dotted) lines cannot be detected with Γ_1^q ($A_{LR}^q + A_{FB}^q$). The ellipses are the combined regions, which cannot be resolved. Thick (thin) lines correspond to $q = c(b)$.

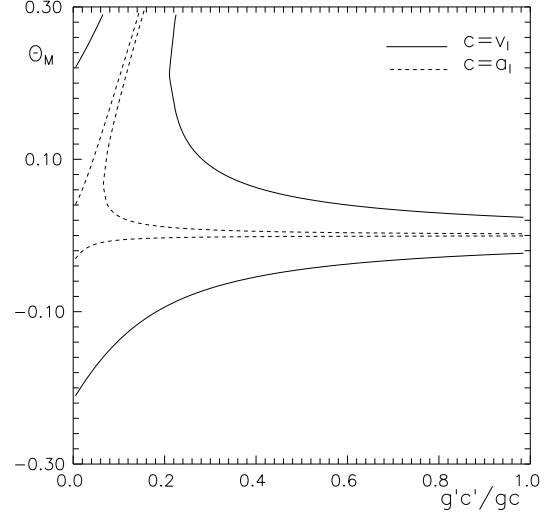


Fig. 4: Areas of $(g'a_l/(ga_l), \theta_M)$ and $(g'v_l/(gv_l), \theta_M)$, for which the extended gauge theory's predictions are indistinguishable from the SM (95% CL). The region containing the line $\theta_M = 0$ cannot be excluded.

Figure 3 shows our results similar to figure 1 but for (a_c^M, v_c^M) and (a_b^M, v_b^M) . The weaker constraints reflect the larger systematic errors of the quark measurements. We used $\Gamma_1^b = R_b \Gamma_{had} = (379.7 \pm 1.9) MeV$ and $\Gamma_1^c = R_c \Gamma_{had} = (299.0 \pm 9.8) MeV$ as input [8]. In contrast to figure 1, the uncertainty of the exclusion region due to ρ_{mix} is negligible here. The missing constraint from $A_{LR}^b + A_{FB}^b$ at one side is due to the theoretical prediction, which is too close to one to allow for a $\chi^2 = 5.99$ even for $A_b = 1$ with the given experimental error.

Model dependent fits constrain θ_M using hadronic and leptonic observables simultaneously. Furthermore, there are less Z' parameters to be determined in such a fit. As a result, the model dependent Z' limits are better than those obtained for the same model from the model independent constraints as demonstrated above. Numerically, the difference can be estimated, for example, comparing the limit for the χ model $-0.006 < \theta_M < 0.008$ taken from figure 3 of the first reference in [2] for $M_{Z'} = 700 GeV$ with the range $|\theta_M| < 0.04$, which would be obtained by our model independent analysis using Γ_1^l and A_{FB}^l from the same data set of the analysis [2].

The limits on a_e^M and v_e^M obtained from LEP 1 data can be compared with future constraints from $e^+e^- \rightarrow W^+W^-$. The rectangle in figure 1 is calculated from figure 1 of reference [6] where the constraint on the anomalous couplings $g_{WW\gamma}^* = 1 + \delta_\gamma$ and $g_{WWZ}^* = \cot \theta_W + \delta_Z$ is plotted for $\sqrt{s} = 500 GeV$ and $L_{int} = 50 fb^{-1}$. For small ZZ' mixing and $M_{Z'}^2 \gg s$, the values δ_γ and δ_Z are linearly related to a_e^M and v_e^M ,

$$\delta_Z = \cot \theta_W \cdot \frac{a_e^M}{ag}, \quad \delta_\gamma = \cot \theta_W \cdot v_e \left(\frac{a_e^M}{ga} - \frac{v_e^M}{gv} \right) \chi, \quad \chi = \frac{s}{s - M_Z^2}. \quad (14)$$

The constraint on a_q^M and v_q^M from the Z_1 peak cannot be improved by W pair production.

The model independent limits in figure 1 can be interpreted as constraints on a weakly coupling Z' . Explore that figure 1 depends only on the *combinations* $\theta_M g' a'_l$ and $\theta_M g' v'_l$. Then, we obtain for sufficiently small θ_M the constraint on θ_M for a Z' model with a “scaled” coupling strength $g' \rightarrow \lambda g'$ as $\theta_M \rightarrow \theta_M/\lambda$. In the simplest approximation where only the linear terms in θ_M are kept in equation (3), we obtain

$$|\theta_M| < \frac{\Delta c}{c} \frac{gc}{g'c'}, \quad \text{where } c = a_l, v_l. \quad (15)$$

Δc is the bound on a'_l or v'_l obtained from figure 1, i.e. $\Delta v_l = 0.0008$ and $\Delta a_l = {}^{+0.0003}_{-0.0011}$. The exact numerical result is shown in figure 4. The approximate bound (15) is recovered for large $g'c'/(gc)$. In contrast to (15), the exact calculation gives a bound on θ_M also for a Z' with zero coupling, i.e. for $g'c'/(gc) = 0$. It is $|\theta_M| < 0.034$ for $c = a_l$. The existence of such a bound can easily be understood from equation (3), where the deviation of the coupling $a_f(1)$ or $v_f(1)$ from a_f or v_f with increasing θ_M eventually becomes larger than the experimental error, even in the case $g' = 0$. If one allows for a large ZZ' mixing, there is one particular Z' with *all* couplings proportional to those of the SM Z boson and a proper overall coupling strength,

$$g'c'_f = gc_f \frac{1 - \cos \theta_M}{\sin \theta_M}, \quad c = a, v, \quad (16)$$

which would produce no deviation of $c_f(1)$ from c_f . The begin of this second region of insensitivity (besides the region $\theta_M \approx 0$) can be recognized for small $g'c'/(gc)$ in figure 4. Such a special model could be detected only by effects of the Z_2 propagator. If equation (16) is fulfilled for a'_l , but not for v'_l , the curve for v'_l in figure 4 would constrain the ZZ' mixing. Considerations similar to figure 4 can be made for the couplings of the Z' to quarks.

To summarize, we demonstrated in a simple analysis how model independent Z' limits based on the data from the Z_1 peak could be obtained. The constraints on $a_c^M, v_c^M, a_b^M, v_b^M$ are unique, while the constraints on a_e^M and v_e^M could be improved by measurements of $e^+e^- \rightarrow W^+W^-$ at energies beyond LEP 2. The relation between model independent and model dependent Z' constraints was discussed. It was pointed out that LEP data set bounds on the ZZ' mixing angle even for a Z' with arbitrary small couplings.

In our simple analysis, we neglected correlations between the different measurements and assumed that the SM parameters remain unchanged in a Z' fit. In a more realistic analysis, the SM model parameters and the model independent Z' parameters a_f^M, v_f^M should be determined simultaneously and all correlations should be taken into account.

Acknowledgments

I would like to thank W. Hollik, A. Pankov and T. Riemann for discussions.

References

- [1] J. Layssac, F.M. Renard and C. Verzegnassi, Z. Physik **C53** (1992) 97;
 J. Layssac, F.M. Renard and C. Verzegnassi, Phys. Lett. **B287** (1992) 267;
 P. Langacker, M. Luo, Phys. Rev. **D45** (1992) 278;
 L3 collaboration, Phys. Lett. **B306** (1993) 187;
 G. Altarelli, et al., Phys. Lett. **B318** (1993) 139.

- [2] A. Leike, S. Riemann, T. Riemann, Phys. Lett. **B291** (1992) 187;
A. Leike, S. Riemann, Nucl. Phys. **B** (Proc. Suppl.) **29A** (1992) 270.
- [3] S. Riemann, L3 Note 1961, 1996.
- [4] A. Leike, Z. Phys. **C62** (1994) 265.
- [5] A. Leike, S. Riemann, preprint DESY 96-111, LMU-02/96, hep-ph/9607306, to appear in Z. Phys. **C**.
- [6] A.A. Pankov, N. Paver, preprint IC/96/175, UTS-DFT-96-01, hep-ph/9610509.
- [7] W. de Boer, A. Dabelstein, W. Hollik, W. Möhle, U. Schwickerath, IEKP-KA/96-08 (revised version), hep-ph/9609209.
- [8] A. Blondel, Plenary talk at 28th Int. Conf. on High Energy Physics, Warsaw, July 1996; LEP Electroweak Working Group, CERN-preprint LEPEWWG/96-02.
- [9] A. Akhundov, D. Bardin, T. Riemann, Nucl. Phys. **B276** (1986) 1.
- [10] C. Bardin, et al., ZFITTER description, CERN-TH. 6443/92.
- [11] W. Hollik, Karlsruhe preprint KA-TP-24-1996.
- [12] For a review see e.g. J.L. Hewett, T.G. Rizzo, Phys. Rep. **183** (1989) 193.
- [13] L.S. Durkin, P. Langacker, Phys. Lett. **B166** (1986) 436.
- [14] For a review see e.g. R.N. Mohapatra, “Unifications and Supersymmetries”, (Springer, New York, 1989).